# An assessment of structural enthalpy and crystallisation pathways of $Mg_{65}Zn_{30}Ca_5$ bulk metallic glass and amorphous films

**Scott Gleason, David Miskovic, Nicholas Hamilton, Kevin Laws, Michael Ferry**

UNSW Australia
School of Material Science and Engineering

August 30, 2017

# ABSTRACT

The structural nature and thermal stability of amorphous alloys is highly dependent on the method by which they are produced, i.e. their relaxation rate upon cooling. Both bulk samples and metallic glass films of $Mg_{65}Zn_{30}Ca_5$ were produced by copper mold casting and direct current (DC) magnetron sputtering onto aluminium substrates, respectively. Comparisons between structural enthalpy, crystallisation pathways, relaxation and crystallisation kinetics of the bulk samples and films were examined by elevated temperature XRD and DSC. Compared with equivalent experiments on the bulk alloy, results for the thin films show distinct differences in structural enthalpy and deviations from the expected crystalline phase evolution, displaying minor peak shifts, failure of some phases to evolve, and variations in the evolution rates.

# TABLE OF CONTENTS

# 1 INTRODUCTION

The structural nature and thermal stability of amorphous alloys is highly dependent on the method by which they are produced, i.e. their relaxation rate upon cooling. Both bulk samples and metallic glass films of $Mg_{65}Zn_{30}Ca_5$ were produced by copper mold casting and direct current (DC) magnetron sputtering onto aluminium substrates, respectively. Comparisons between structural enthalpy, crystallisation pathways, relaxation and crystallisation kinetics of the bulk samples and films were examined by elevated temperature XRD and DSC. Compared with equivalent experiments on the bulk alloy, results for the thin films show distinct differences in structural enthalpy and deviations from the expected crystalline phase evolution, displaying minor peak shifts, failure of some phases to evolve, and variations in the evolution rates.

# 2 METHOD

## 2.1 Master alloy

The master alloy of $Mg_{65}Zn_{30}Ca_5$ was produced using high-purity elements of Mg (99.85 wt%), Zn (99.995 wt%), and Ca (99.8 wt%). The alloy was prepared with an in-house induction melting furnace within boron nitride coated graphite crucibles, purged with Ar (99.997 vol.% purity) five times, and protected with a circulating Ar atmosphere. Alloy homogeneity was ensured by heating and cooling through a cycle of 700°C, 385°C, 650°C, 385°C, 650°C to a casting temperature of 500 °C and 450°C for injection and gravity casting respectively. Bulk amorphous $Mg_{65}Zn_{30}Ca_5$ rods of nominal $2.5mm$ diameter sectioned to $1mm$ thickness, and plates of nominal $1.2mm$ thickness were produced by copper mold injection casting. The $25.4mm$ diameter targets were prepared from cylindrical copper mold gravity castings sectioned to nominal thicknesses of $3.25mm$, and polished. All samples and targets were stored under Ar when not being examined or used.

## 2.2 DC magnetron sputtering

Films were produced from an in-house DC magnetron sputtering facility with Ar working gas (99.997 vol.% purity). The power was $15W$, typical voltage of $285 - 325V$, nominal chamber pressure of 1 bar, substrate temperature of 25°C, and Ar flow of 3.01 SCCM. Films were deposited directly onto to Al DSC lid substrates. Depositions were for a period of 35 minutes at an estimated deposition rate of $0.8nm/s$.

## 2.3 Stylus profiler analysis

Nominal film thickness was measure by a stylus profiler (Dektak 2A, Bruker, Germany). A glass slide was placed under the substrates within the sputtering chamber, allowing the substrates to act as a mask. Profile measurements were taken by measuring the height difference between the bare glass and the film coated glass. This film thickness was used to estimate the sputter deposition rate.

## 2.4 EDS analysis

Alloy composition and homogeneity were confirmed by SEM-EDS (S3400-N, Hitachi, Japan; Nova NanoSEM 230/450, FEI, The Netherlands). Hyper-maps were collected with an accelerating voltage of $15-20keV$, a probe current of $50\mu A$, spot size 4.2, counts of $5000cps$ or better, dead time less than 20%, and working distance was $5mm$.

## 2.5 DSC characterization

Isochronic DSC (204 F1 Phoenix, Netzsch, Selb, Germany) was carried out in Al crucibles under a protective Ar atmosphere (99.997 vol.% purity). Scans were performed at heating rates ($\beta$s) of 5 to $100K/min$.

Isothermal relaxation acrshortdsc was preformed by heating samples at $20K/min$ to the desired annealing temperature, holding for the desired time, and Ar quenching to room temperature.

For annealed XRD the samples were heat treated in the DSC by heating to the desired temperature at $20K/min$ followed by Ar quenching to room temperature.

## 2.6 XRD characterization

Annealing XRD (Empyrean, PANalytical, Cu $K_\alpha$ X-ray source, $\lambda = 1.541$Å) was performed on heat treated bulk rods and films at room temperature. With a generator voltage $45kV$, tube current $40mA$, scan step size 0.0262606, and time per step of 397.29.

Dynamic XRD (D8, Bruker, Cu $K_\alpha$ X-ray source, $\lambda = 1.541$Å) was performed on as manufactured bulk plates and films by raising temperature at a rate of $20K/min$ and performing scans *in situ*. The first scan was performed at 35°C, then 75°C, after which temperature was raised in 5°C increments until reaching a final temperature at 185°C. The $2\theta$

scans from $31 - 60^\circ$ were completed within $1092sec$ ($18min$, $12sec$) to minimise the effects of recrystallisation during the experiment. With a generator voltage $45kV$, tube current $100mA$, scan step size 0.02, and time per step of 134.4.

# 3 RESULTS

## 3.1 Alloy composition

From the 35 minute depositions a nominal film thickness of $1.64 \pm 0.48\mu m$ was obtained, giving a deposition rate of approximately $0.81 \pm 0.22nm/s$. The substrate temperature within the chamber was found to rise $2.9 - 3.5°C$, significantly less than the expected $20K$ suggested by similar setups [1], see Figure 1.

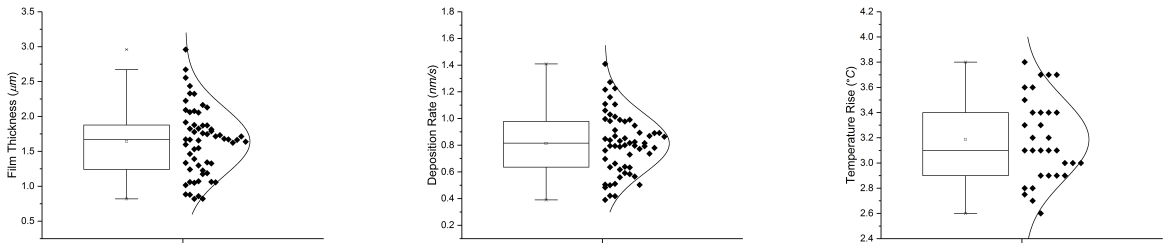


(a) (b) (c)

Figure 1: (a) Box and whisker plot of the measured film thicknesses from depositions. (b) Box and whisker plot of the calculated deposition rates achieved. (c) Box and whisker plot of substrate temperature rise.

EDS analysis shows good agreement in the nominal composition for both the bulk and film $Mg_{65}Zn_{30}Ca_5$, see Table 1.

Table 1: EDS composition of bulk and film $Mg_{65}Zn_{30}Ca_5$ in atomic weight percent.

| EDS Analysis | Bulk (at%) | Film (at%) |
|---|---|---|
| Mg | $64.92 \pm 3.22$ | $63.20 \pm 3.28$ |
| Zn | $29.55 \pm 0.84$ | $30.95 \pm 0.96$ |
| Ca | $5.53 \pm 0.17$ | $5.85 \pm 0.19$ |

## 3.2 DSC

### 3.2.1 Isochronic DSC

Isochronic DSC was performed on the bulk and film $Mg_{65}Zn_{30}Ca_5$ to examine the thermal properties. The bulk alloy was relaxed at 120°C for 10 minutes before DSC measurements to ensure the glass transition temperature ($T_g$) was clearly visible. The film was not relaxed as unlike the bulk the lost in free volume from relaxation would be significant and make differences between the samples much more difficult to observe [source needed???].

The bulk $Mg_{65}Zn_{30}Ca_5$ was examined at heating rates ($\beta$s) of 5, 10, 15, 20, 30, 40, 60, 80, and 100 $K/min$ to observe changes in the $T_g$ and crystallisation temperatures ($T_x$s) with $\beta$. As expected greater $\beta$ resulted in greater signal strength, exothermic peaks shifting to higher start temperatures, and an increase in thermal lag resulting in later exothermic finish temperatures and curve convolution. With this convolution the $T_g$ and $T_{x1}$ remained clearly visible for all $\beta$s, but $T_{x2,4,5}$ were only visible at low $\beta$s, and $T_{x3}$ was not clear at any $\beta$, see Figure 2.

The film was examined at $\beta$s of 15, 20, 30, 40, 60, 80, and 100 $K/min$. The lower $\beta$s of 5 and 10 $k/min$ were not utilised owing to the lower film signal compared to the bulk. The reduced signal was likely from the low mass of the film, about $\frac{1}{10}$ that of the bulk. The film showed the expected variable relationships with increasing $\beta$ as observed in the bulk. The signal intensity increased at a compatible rate to bulk up until $\beta$s of 80 and 100 $k/min$. These final two $\beta$s showed great increases in the signal intensity. The exothermic peaks all convoluted together making many of the thermodynamic events difficult to observer at all $\beta$s. It also appeared that all exothermic events shifted to lower temperatures as compared to the bulk. The film $T_g$ and $T_{x1}$s were less defined than for the bulk, but could still be identified for all $\beta$s. For all $\beta$s the $T_{x2-5}$ onsets could not be easily identified, see Figure 3.

### 3.2.2 Fragility

Using the isochronic DSC $T_g$s the fragility ($m$) of the $Mg_{65}Zn_{30}Ca_5$ system could be established for both the bulk and film. Numerical solutions where used to fit the DSC variant of the Vogel–Fulcher–Tammann (VFT) relationship for $\beta$ [2].

$$\beta^{-1} = \tau_0 \, e^{\left(\frac{D^* T_0}{T_g - T_0}\right)} \tag{1}$$

Where $\tau_0$ is a pre-exponential factor, $D^*$ is the liquid fragility parameter, and $T_0$ is the VFT temperature where the barrier to flow becomes infinite.

The $m$ could then be calculated from Equation 2 [3, 4].

$$D^* = 590/(m - 16) \tag{2}$$

Using these two equations for the bulk it was found $\beta^{-1} = 1.338E - 16e^{5274(\frac{1}{T-T_0})}$ with an Adj. $R^2 = 0.972$. This gave a $D^* = 20.4$, and a $m$= 44.9. The film was fitted to $\beta^{-1} = 5.921E - 11e^{2766(\frac{1}{T-T_0})}$ with a lower confidence of Adj. $R^2 = 0.861$, likely owing to the reduced number of data points. This gave a $D^* = 10.0$, and $m$= 75.0, see Figure 4.

## 3.3 DSC deconvolution

### 3.3.1 Onset determination

Numerical solutions were used to deconvolute the isochronic DSC curves so the various $T_x$ onsets could be accurately determined. This numerical fitting utilised a summation of skewed Gaussian curves to fit a target curve corresponding to the original data; as is a common method [5–9]. For simplified, un-skewed peaks this fitting summation takes the form of Equation 3.

$$f(x) = \sum_{n=i}^{n} h_i \, e^{-}\left(\frac{(x - T_i)^2}{(2c_j)^2}\right) \tag{3}$$

Where $h$ is the magnitude of the enthalpy peak, $T$ is the temperature at the enthalpy peak centre, and $c$ is the Gaussian RMS width.

The final deconverged solutions of this fitting for both the bulk and film are shown in Figures 5 and 6 respectively. These results are tabulated in Table 2 for the bulk and Table 3 for the film. Tables 2 and 3 are also plotted together in Figure 7 with the bulk shown in black and the film in red. Note the $T_g$ and $T_{x1}$ are obtained from the original raw data, not the deconvolution.

It is worth noting the deconvolution fitted 5 crystallisation events for the bulk $Mg_{65}Zn_{30}Ca_5$, but only 3 events for the film. This occured because the bulk had 5 well defined events, where as the film was largely convoluted together. Thus unique solutions could not be obtained for the lesser $T_{x2}$ and $T_{x4}$ events of the film.

Table 2: Bulk $Mg_{65}Zn_{30}Ca_5$ alloy onset temperatures for the various DSC heating rates ($\beta$s). All temperatures are in °C.

| Heating Rate $\beta$ $K/min$ | $T_g$ °C | $T_{x1}$ °C | $T_{x2}$ °C | $T_{x3}$ °C | $T_{x4}$ °C | $T_{x5}$ °C |
|---|---|---|---|---|---|---|
| 100 | 136.1 | 164.8 | 193.4 | 201.8 | 240.2 | 262.4 |
| 80 | 132.0 | 160.0 | 194.4 | 201.9 | 238.2 | 260.3 |
| 60 | 129.6 | 157.7 | 190.0 | 197.8 | 232.9 | 259.0 |
| 40 | 126.6 | 155.2 | 189.0 | 200.0 | 226.4 | 254.7 |
| 30 | 126.2 | 151.5 | 187.0 | 198.4 | 221.0 | 251.1 |
| 20 | 125.1 | 149.8 | 188.4 | 197.0 | 216.0 | 246.8 |
| 15 | 123.8 | 148.3 | 186.2 | 195.6 | 212.2 | 243.9 |
| 10 | 123.5 | 144.5 | 183.4 | 192.9 | 207.4 | 239.8 |
| 5 | 120.5 | 141.1 | 179.7 | 187.5 | 199.8 | 232.7 |

Table 3: Film $Mg_{65}Zn_{30}Ca_5$ alloy onset temperatures for the various DSC heating rates ($\beta$s). All temperatures are in °C.

| Heating Rate $\beta$ $K/min$ | $T_g$ °C | $T_{x1}$ °C | $T_{x2}$ °C | $T_{x3}$ °C | $T_{x4}$ °C | $T_{x5}$ °C |
|---|---|---|---|---|---|---|
| 100 | 108.5 | 128.6 | | 177.3 | | 240.3 |
| 80 | 106.0 | 121.2 | | 165.6 | | 238.8 |
| 60 | 107.3 | 134.0 | | 176.1 | | 237.8 |
| 40 | 100.2 | 119.8 | | 170.7 | | 234.2 |
| 30 | 95.3 | 110.4 | | 169.5 | | 232.5 |
| 20 | 95.5 | 115.2 | | 170.5 | | 229.4 |
| 15 | 92.5 | 113.5 | | 168.8 | | 224.0 |

### 3.3.2 Reaction enthalpy

The deconvolution fits were integrated to find the area under each curve. This information provides the specific enthalpy ($h$) of the crystallisation formation of each phase. These energies are presented in Tables 4 and 5 for the bulk and film respectively. Figure 8 shows the $T_x$ onsets and specific enthalpy ($h$) for both the bulk and film plotted together.

From Tables 4 and 5, and Figure 8 it can be seen most of the crystallisation formation energy is needed to form the $1^{st}$, $3^{rd}$, and $5^{th}$ phases (i.e. $T_{x1,3,5}$). With these three phases accounting for approximately $73 \pm 7\%$ of the bulk crystallisation energy. The total crystallisation energy of these three bulk phases is also similar to the total energy for the films. Demonstrating that the bulk requires more energy to crystallize than the films.

This is v
scientist
expected
glass. i.e
expectat

Table 4: Bulk $Mg_{65}Zn_{30}Ca_5$ alloy specific enthalpy ($h$) of crystallisation formation for $Tx_{1-5}$ for the various DSC heating rates ($\beta$s); $h$ is in $J/g$.

| Heating Rate $\beta$ $K/min$ | $h_{T_{x1}}$ $J/g$ | $h_{T_{x2}}$ $J/g$ | $h_{T_{x3}}$ $J/g$ | $h_{T_{x4}}$ $J/g$ | $h_{T_{x5}}$ $J/g$ | $h_{Total}$ $J/g$ |
|---|---|---|---|---|---|---|
| 100 | 59.59 | 6.97 | 49.16 | 22.84 | 46.08 | 184.64 |
| 80 | 42.61 | 6.08 | 32.33 | 18.27 | 31.25 | 130.54 |
| 60 | 30.02 | 4.05 | 25.41 | 16.76 | 19.81 | 96.05 |
| 40 | 16.93 | 4.36 | 12.44 | 11.13 | 11.68 | 56.54 |
| 30 | 12.03 | 3.68 | 9.32 | 9.18 | 9.02 | 43.23 |
| 20 | 7.18 | 2.21 | 4.99 | 5.67 | 5.78 | 25.83 |
| 15 | 5.48 | 2.01 | 3.65 | 4.69 | 4.43 | 20.26 |
| 10 | 3.45 | 1.43 | 2.28 | 3.14 | 2.92 | 13.22 |
| 5 | 1.65 | 0.69 | 1.09 | 1.47 | 1.42 | 6.32 |

Table 5: Film $Mg_{65}Zn_{30}Ca_5$ alloy specific enthalpy ($h$) of crystallisation formation for $Tx_{1-5}$ for the various DSC heating rates ($\beta$s); $h$ is in $J/g$.

| Heating Rate $\beta$ $K/min$ | $h_{T_{x1}}$ $J/g$ | $h_{T_{x2}}$ $J/g$ | $h_{T_{x3}}$ $J/g$ | $h_{T_{x4}}$ $J/g$ | $h_{T_{x5}}$ $J/g$ | $h_{Total}$ $J/g$ |
|---|---|---|---|---|---|---|
| 100 | 48.24 | | 49.85 | | 43.38 | 141.47 |
| 80 | 43.27 | | 53.56 | | 36.18 | 133.01 |
| 60 | 15.5 | | 8.78 | | 22.4 | 46.68 |
| 40 | 16.22 | | 9.13 | | 16.27 | 41.62 |
| 30 | 13.72 | | 7.16 | | 11.81 | 32.69 |
| 20 | 6.16 | | 2.3 | | 7.45 | 15.91 |
| 15 | 6.99 | | 3.66 | | 6.57 | 17.22 |

### 3.3.3 Relaxation enthalpy

For next paper on relaxation / rejuvenation.

## 3.4 XRD

### 3.4.1 Annealing XRD

The crystallisation events observed and deconvoluted from the DSC were further examined with annealing XRD. Both the bulk and film were heat treated by annealing to 120, 140, 145, 170, 200, 250, 290, and 320°C before XRD. This allowed for the location of the $T_g$ and $T_x$s to be confirmed as well as for the crystallisation phases to be identify.

From these experiments 5 previously observed crystallisation phases of the MgZnCa system [10–14] were characterised in the bulk and film $Mg_{65}Zn_{30}Ca_5$. This allowed the

crystallisation process of $Mg_{65}Zn_{30}Ca_5$ from the fully amorphous glass to fully crystalline metal to be identified as;

$$\text{Glass} \rightarrow Mg_{51}Zn_{20} \rightarrow \text{Mg} \rightarrow Ca_2Mg_5Zn_5 \rightarrow \text{MgZn} \rightarrow Ca_2Mg_5Zn_{13}$$

The annealing XRD results are shown in Figures 9 and 10 for the bulk and film respectively. In these figures each phase is identified with a tracer at the temperature it was most strongly observed. Note the Al substrates peaks have been faceted in Figure 10 as to not dwarf the other peaks.

In Figures 9 and 10 it can be observed that $Mg_{51}Zn_{20}$ and Mg come out at a lower temperature in the film compared to the bulk, while the other phases nucleate and grow at similar rates for both the bulk and film. The temperature each phase is first and last observed are tabulated in Table 6.

Note the phases identified in Table 6 have reasonable agreement with the $T_g$ and $T_x$ onset temperatures presented in Tables 2 and 3. With $Mg_{51}Zn_{20}$ and Mg corresponding to either $T_{x1}$ or $T_{x2}$, $Ca_2Mg_5Zn_5$ to $T_{x3}$, MgZn to $T_{x4}$, and $Ca_2Mg_5Zn_{13}$ to $T_{x5}$.

Table 6: Temperatures at which each crystallisation phase is first and last observed in the annealing XRD for both the bulk and film. All temperatures are in °C.

| Phase | Bulk | | Film | |
|---|---|---|---|---|
| | First Temp | Last Temp | First Temp | Last Temp |
| Glass | 35 | 200 | 35 | 200 |
| $Mg_{51}Zn_{20}$ [10, 13] | 170 | 200 | 140 | 200 |
| Mg | 170 | 320 | 140 | 320 |
| $Ca_2Mg_5Zn_5$ [10, 14] | 200 | 250 | 200 | 250 |
| MgZn [13] | 250 | 250 | 250 | 250 |
| $Ca_2Mg_5Zn_{13}$ [10–12] | 290 | 320 | 290 | 320 |

### 3.4.2 Dynamic XRD

The annealing XRD was useful for identifying the crystal phases present, but not many differences between the evolution rates of the bulk or film could be observed. Thus samples were subjected to dynamic XRD over their most active $2\theta$ range of $31 - 60°$ to observe changes *in-situ*. This allowed the crystallisation to be actively observed over the range of $35 - 185$°C, showing how phases evolved over time as the temperature was raised in 5°C increments.

The dynamic XRD data shows that many phases seen in the bulk nucleate at different temperatures, are not observed as strongly, or fail to nucleate in the film. The initial Mg and $Mg_{51}Zn_{20}$ peak at $32.1°$ is first clearly seen in the bulk at a temperature of 170°C. In

the film the first clear evidence of this peak is at 90°C, although its resolution is poor from 150-170°C. The Mg, $Mg_{51}Zn_{20}$, and $Ca_2Mg_5Zn_5$ peak at 34.3° is seen at 75°C in the bulk, but not till 115°C in the film. The Mg and $Mg_{51}Zn_{20}$ peak at 47.7° is seen in both the bulk and film at 170°C.

In the bulk a double peak at 38° and 39° begins to emerge at 125°C, phases which never evolve in the film. The bulk $Ca_2Mg_5Zn_5$ peaks at 42.3° and 43.7° start to emerge at 165°C and 170°C respectively, but are never seen in the film. A faint $Mg_{51}Zn_{20}$ and $Ca_2Mg_5Zn_5$ peak at 53.3°is seen in the bulk at 175°C, but never in the film. The final small Mg and $Mg_{51}Zn_{20}$ 57.2° peak at 170°C is also never seen in the film. These observations are tabulated in Table 7. The bulk dynamic XRD is shown in Figure 11, and the film in Figure 12. Normalised plots allowing for easy identification of differences between the bulk and film are shown in Figures 13, 14, and 15.

Table 7: Main dynamic XRD peaks for both the bulk and the film. Data shows minor shifting for peaks 3 and 8, large start temperature differences for peaks 1 and 2, and failure of peaks $4-7$, 9, and 10 to nucleation in the film.

| Peak | Bulk $2\theta$ | Film $2\theta$ | Change % | Bulk Start °C | Film Start °C | Change % | Phases at% |
|---|---|---|---|---|---|---|---|
| 1 | 32.1 | 32.1 | 0.0% | 170 | 90 | -47.1% | Mg, $Mg_{51}Zn_{20}$ |
| 2 | 34.3 | 34.3 | 0.0% | 75 | 115 | 53.3% | Mg, $Mg_{51}Zn_{20}$, $Ca_2Mg_5Zn_5$ |
| 3 | 36.6 | 36.5 | -0.3% | 130 | 130 | 0.0% | Mg, $Mg_{51}Zn_{20}$ |
| 4 | 38.0 | N/A | N/A | 125 | N/A | N/A | $Mg_{51}Zn_{20}$, $Ca_2Mg_5Zn_5$ |
| 5 | 39.0 | N/A | N/A | 125 | N/A | N/A | $Mg_{51}Zn_{20}$ |
| 6 | 42.3 | N/A | N/A | 165 | N/A | N/A | $Ca_2Mg_5Zn_5$ |
| 7 | 43.7 | N/A | N/A | 170 | N/A | N/A | $Ca_2Mg_5Zn_5$ |
| 8 | 47.7 | 47.6 | -0.2% | 170 | 170 | 0.0% | Mg, $Mg_{51}Zn_{20}$ |
| 9 | 53.3 | N/A | N/A | 175 | N/A | N/A | $Mg_{51}Zn_{20}$, $Ca_2Mg_5Zn_5$ |
| 10 | 57.2 | N/A | N/A | 170 | N/A | N/A | Mg, $Mg_{51}Zn_{20}$ |

It was also observed that there was a some minor peak shifting between the Mg, $Mg_{51}Zn_{20}$, and $Ca_2Mg_5Zn_5$ phases in the dynamic bulk and film XRD. The largest shifts were seen in the $Ca_2Mg_5Zn_5$ 34.6° peak and $Mg_{51}Zn_{20}$ 39.1° peak, with shifts of 1.4% and 1.0% respectively. These shifts are tabulated in Table 8.

# 4 DISCUSSION

The use of a 60K DSC heating rate ($\beta$) compared to the more commonly used 20K rate [sources] shifts peaks for the bulk $Mg_{65}Zn_{30}Ca_5$ alloy about 8 - 15 degrees higher. This higher $\beta$s were used because crystallisation events for the films were difficult to

Table 8: Location of the dynamic bulk and film XRD peaks for the Mg, $Mg_{51}Zn_{20}$, and $Ca_2Mg_5Zn_5$ compounds.

| Mg | | | $Mg_{51}Zn_{20}$ | | | $Ca_2Mg_5Zn_5$ | | |
|---|---|---|---|---|---|---|---|---|
| Bulk | Film | Change % | Bulk | Film | Change % | Bulk | Film | Change % |
| 32.1 | 32.1 | 0.0% | 32.1 | 32.1 | 0.0% | 34.1 | 34.1 | 0.0% |
| 34.3 | 34.3 | 0.0% | 34.3 | 34.3 | 0.0% | 34.6 | 35.1 | 1.4% |
| 36.6 | 36.5 | -0.3% | 36.6 | 36.5 | -0.3% | 36.0 | 35.7 | -0.8% |
| 47.7 | 47.6 | -0.2% | 38.0 | 38.2 | 0.5% | 38.0 | 38.2 | 0.5% |
| 57.2 | 57.1 | -0.2% | 39.1 | 39.5 | 1.0% | 42.3 | 42.2 | -0.2% |
| | | | 45.1 | 45.2 | 0.2% | 43.7 | 43.3 | -0.9% |
| | | | 47.7 | 47.6 | -0.2% | 53.3 | 53.0 | -0.6% |
| | | | 53.3 | 53.0 | -0.6% | | | |
| | | | 57.2 | 57.1 | -0.2% | | | |

differentiation at the lower $\beta$s. Films show little shift to high temperature peaks with increases $\beta$s, but large shifts with relaxation. Bulk show the opposite behaviour, larger peaks shifts with higher $\beta$s and little shift with relaxation.

# 5 CONCLUSIONS

# 6 ACKNOWLEDGEMENTS

Yu Wang for his assistance with XRD experimentation and Rietveld refinement.

# 7 REFERENCES

[1] J. Q. Wang, N. Chen, P. Liu, Z. Wang, D. V. Louzguine-Luzgin, M. W. Chen, and J. H. Perepezko. The ultrastable kinetic behavior of an Au-based nanoglass. *Acta Materialia*, 79(0):30–36, 2014.

[2] R. Busch, W. Liu, and W. L. Johnson. Thermodynamics and kinetics of the Mg65Cu25Y10 bulk metallic glass forming liquid. *Journal of Applied Physics*, 83(8):4134–4141, 1998.

[3] C. A. Angell and S. Borick. Specific heats Cp, Cv, Cconf and energy landscapes of glassforming liquids. *Journal of Non-Crystalline Solids*, 307 - 310:393–406, 2002.

[4] Shuai Wei, Zach Evenson, Isabella Gallino, and Ralf Busch. The impact of fragility on the calorimetric glass transition in bulk metallic glasses. *Intermetallics*, 55:138–144, 2014.

[5] Samir K. Ashour and Mahmood A. Abdel-hameed. Approximate skew normal distribution. *Journal of Advanced Research*, 1(4):341–350, 2010.

[6] Yuzo Yamamoto, Yuichi Inoue, Teruaki Onai, Chikashi Doshu, Hiroshi Takahashi, and Hiroki Uehara. Deconvolution analyses of differential scanning calorimetry profiles of $\beta$-crystallized polypropylenes with synchronized x-ray measurements. *Macromolecules*, 40(8):2745–2750, 2007.

[7] Charles H. Spink. *Differential Scanning Calorimetry*, volume Volume 84, pages 115–141. Academic Press, 2008.

[8] Charles H. Spink. The deconvolution of differential scanning calorimetry unfolding transitions. *Methods*, 76:78–86, 2015.

[9] Balázs Schäffer, Béla Schäffer, and D. Lõrinczy. Decomposition of dsc curves of dairy products with gaussian functions. *Journal of Thermal Analysis and Calorimetry*, 82(2):531–535, 2005.

[10] Y. N. Zhang, G. J. Rocher, B. Briccoli, D. Kevorkov, X. B. Liu, Z. Altounian, and M. Medraj. Crystallization characteristics of the Mg-rich metallic glasses in the Ca-Mg-Zn system. *Journal of Alloys and Compounds*, 552:88–97, 2013.

[11] Yi-Nan Zhang, Dmytro Kevorkov, Xue Dong Liu, Florent Bridier, Patrice Chartrand, and Mamoun Medraj. Homogeneity range and crystal structure of the Ca2Mg5Zn13 compound. *Journal of Alloys and Compounds*, 523:75–82, 2012.

[12] Yi-Nan Zhang, Dmytro Kevorkov, Florent Bridier, and Mamoun Medraj. Experimental study of the Ca-Mg-Zn system using diffusion couples and key alloys. *Science and Technology of Advanced Materials*, 12(2):025003, 2011.

[13] Y. Khan. Dynamic temperature crystallization behaviour of amorphous and liquid Mg70Zn30 alloy. *Journal of Materials Science*, 24(3):963–973, 1989.

[14] Jake D. Cao, Thomas Weber, Robin Schäublin, and Jörg F. Löffler. Equilibrium ternary intermetallic phase in the Mg-Zn-Ca system. *Journal of Materials Research*, 31(14):2147–2155, 2016.

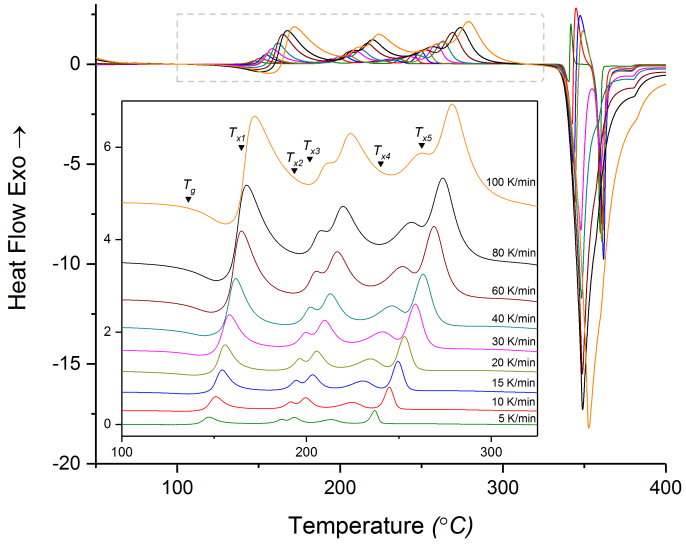


Figure 2: Bulk $Mg_{65}Zn_{30}Ca_5$ relaxed at 120 °C for 10 minutes and heated at various heating rates ($\beta$s) from 5 to $100K/min$. The insert stacks the differential scanning calorimetry (DSC) curves and labels the $T_g$ and $T_x$s of the $\beta = 100K/min$ curve.

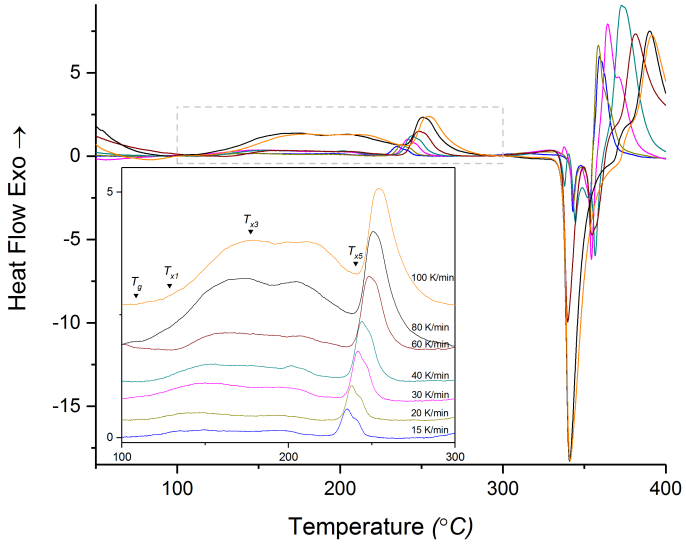


Figure 3: Unrelaxed film $Mg_{65}Zn_{30}Ca_5$ heated at various heating rates ($\beta$s) from 15 to $100K/min$. The insert stacks the DSC curves and labels the $T_g$ and $T_x$s of the $\beta = 100K/min$ curve.

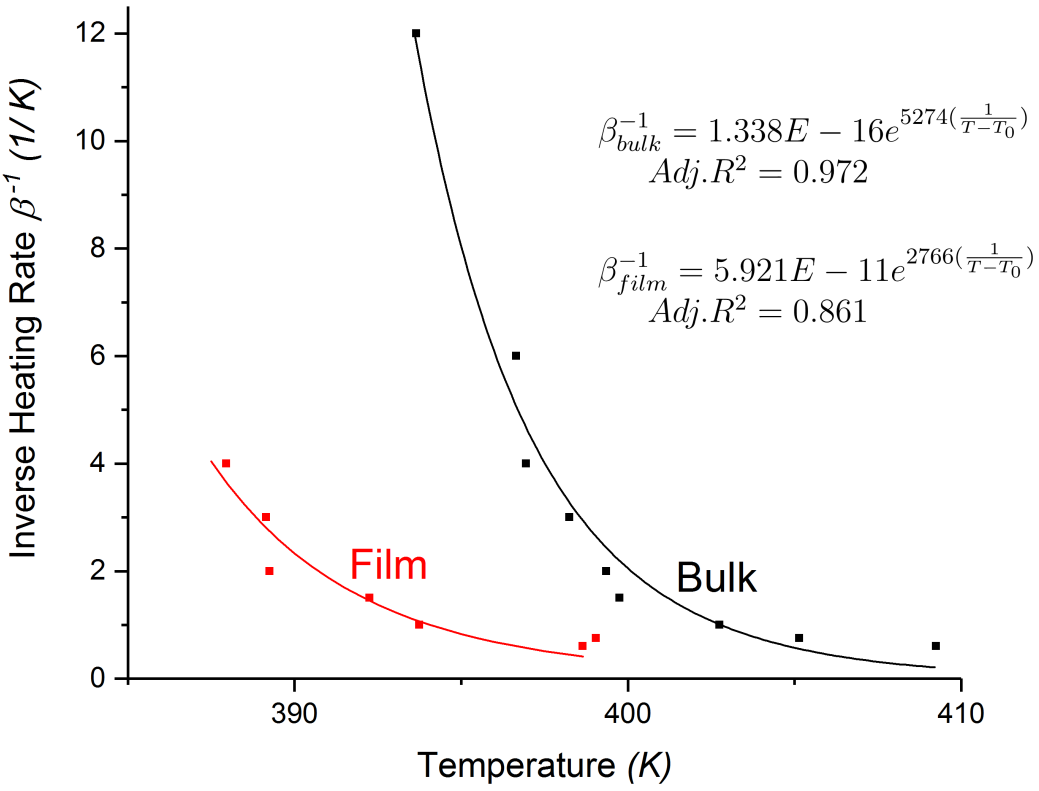


Figure 4: Fitted fragility ($m$) for the $Mg_{65}Zn_{30}Ca_5$ system obtained from the $T_g$ of DSC at various heating rates ($\beta$s) for the bulk and film.

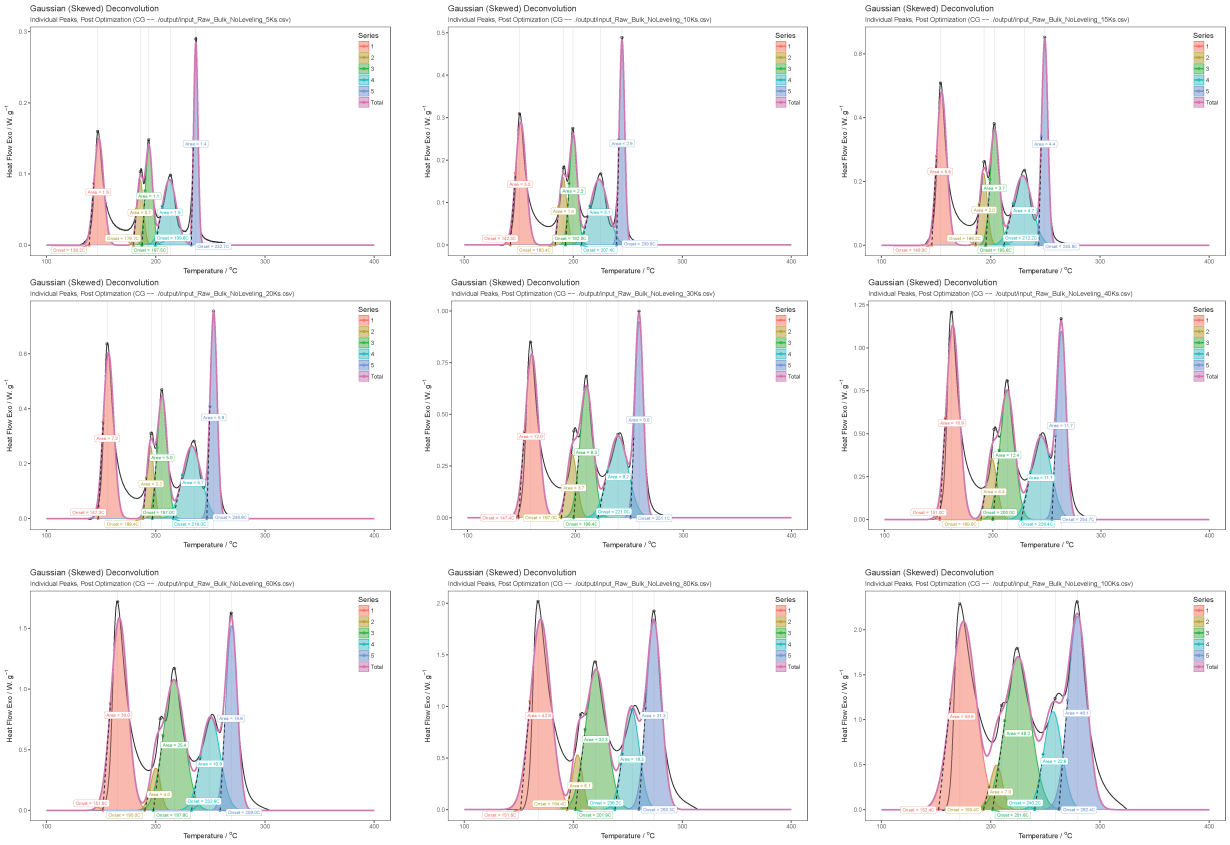


Figure 5: DSC deconvolution for the bulk at various heating rates ($\beta$s). From left to right, top to bottom, $\beta$ = 5, 10, 15, 20, 30, 40, 60, 80, 100 $K/min$.

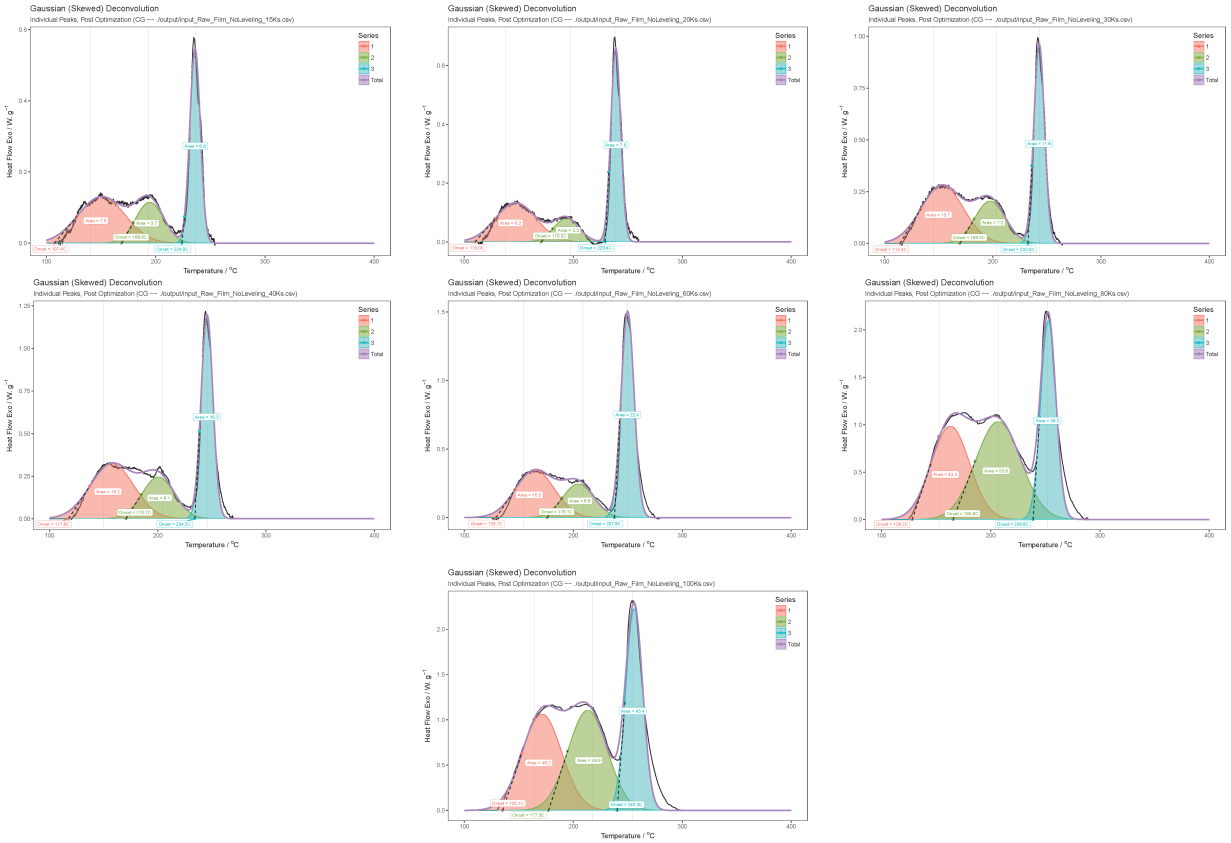


Figure 6: DSC deconvolution for the film at various heating rates ($\beta$s). From left to right, top to bottom, $\beta$ = 15, 20, 30, 40, 60, 80, 100 $K/min$.

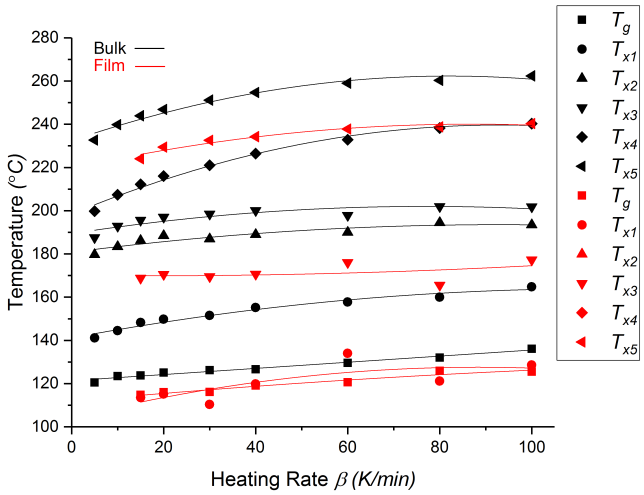


Figure 7: The $T_g$s and $T_x$s plotted at each DSC heating rate ($\beta$) for both the bulk and film $Mg_{65}Zn_{30}Ca_5$. Bulk is shown in black, and film in red.

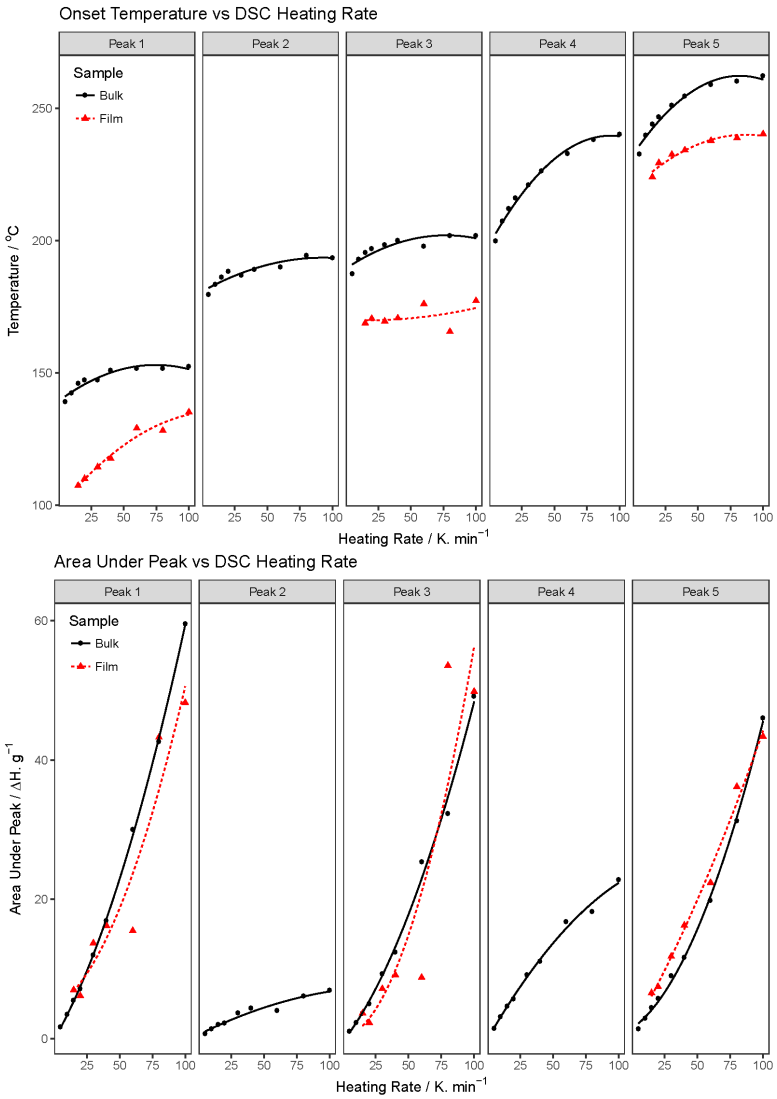


Figure 8: DSC $T_x$ onset temperatures and specific enthalpy ($h$) of crystallisation formation for the bulk and film at each heating rate ($\beta$). Bulk is shown in black, and film in red.

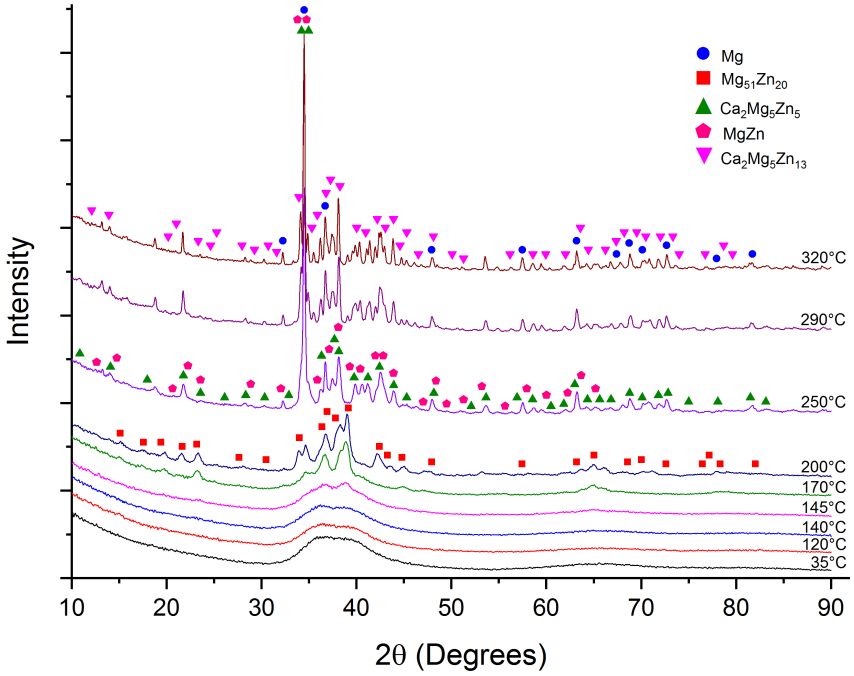


Figure 9: XRD pattern for bulk $Mg_{65}Zn_{30}Ca_5$ heated treated to several temperatures for crystallisation peak identified from DSC. Each phase is identified by a tracer at the temperature it was most strongly observed.

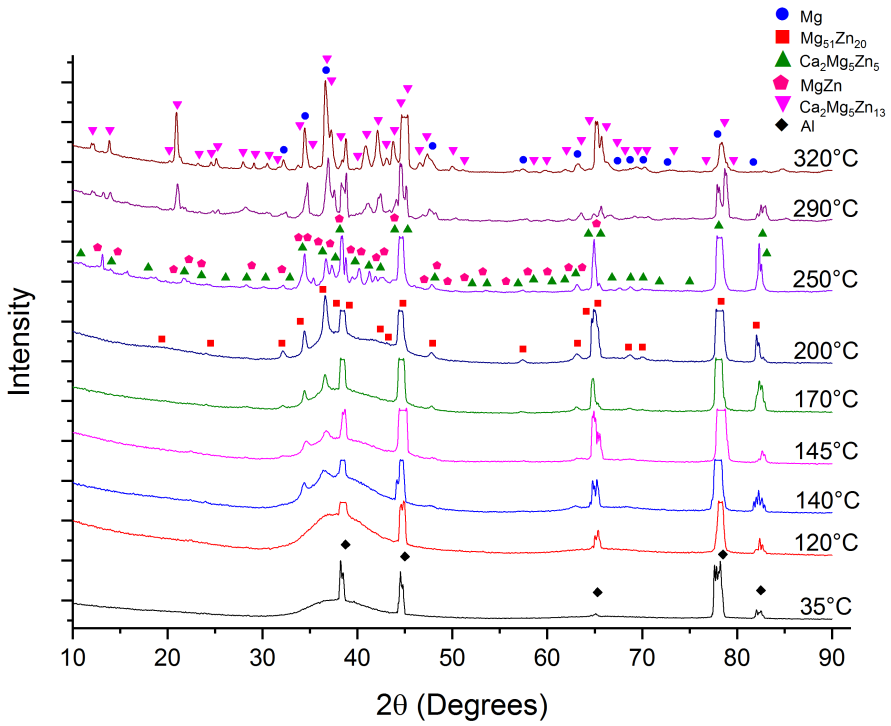


Figure 10: XRD pattern for film $Mg_{65}Zn_{30}Ca_5$ heated treated to several temperatures for crystallisation peak identified from DSC. Each phase is identified by a tracer at the temperature it was most strongly observed. Note the Al substrate peaks have been faceted as to not dwarf all other peaks.

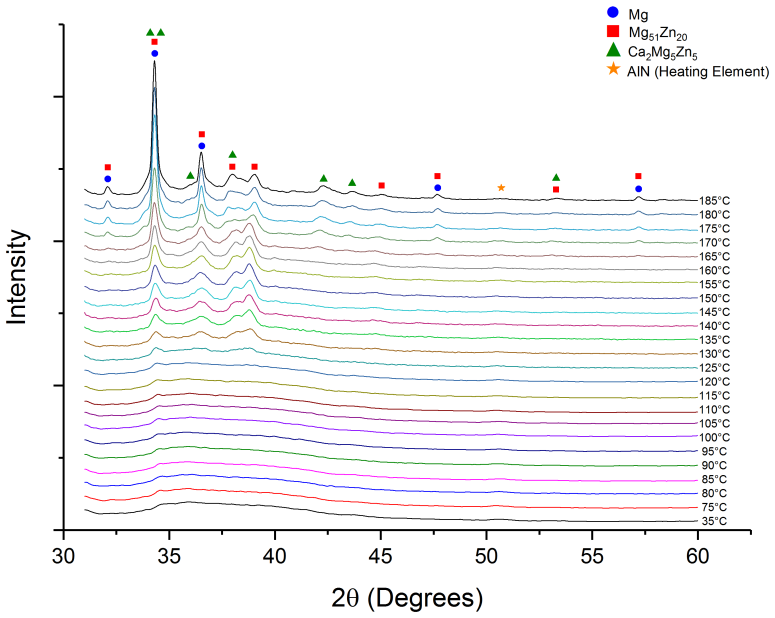


(a)

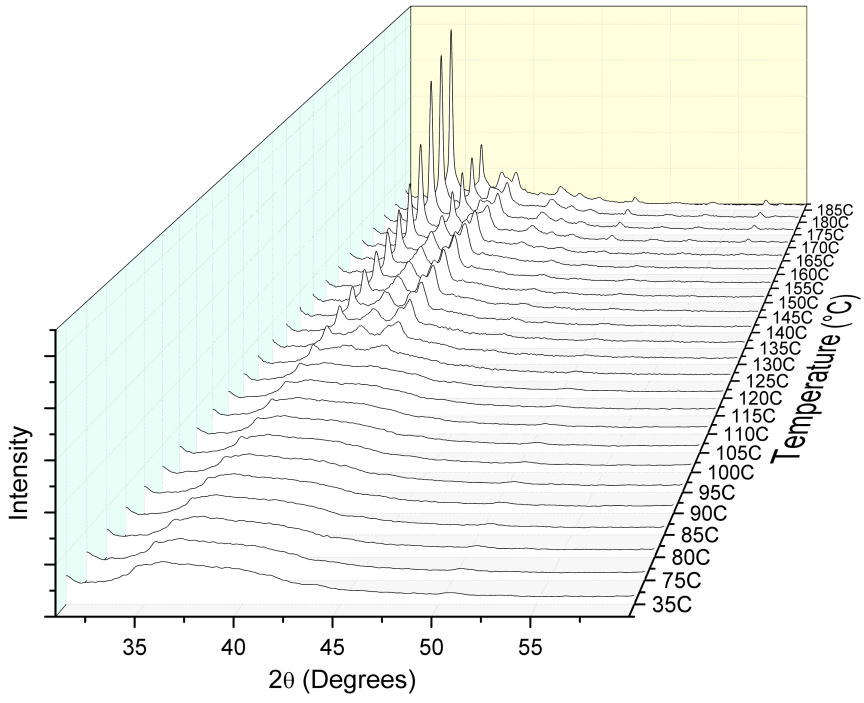


(b)

Figure 11: (a) Stacked XRD patterns from the incremental dynamic *in-situ* heating of bulk $Mg_{65}Zn_{30}Ca_5$. Note the peak around 51° is attributed to the AlN heating element. (b) The same XRD patterns as (a) presented in a cascading layout.

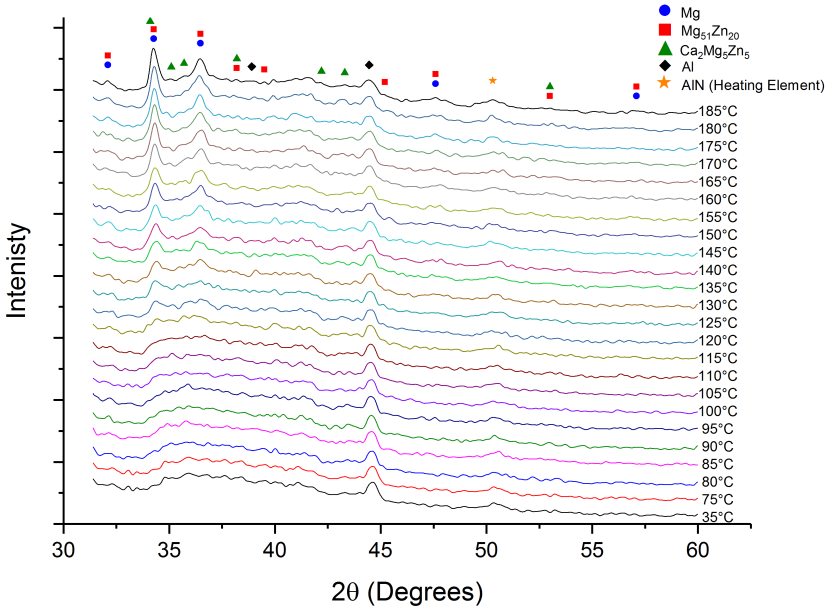


(a)

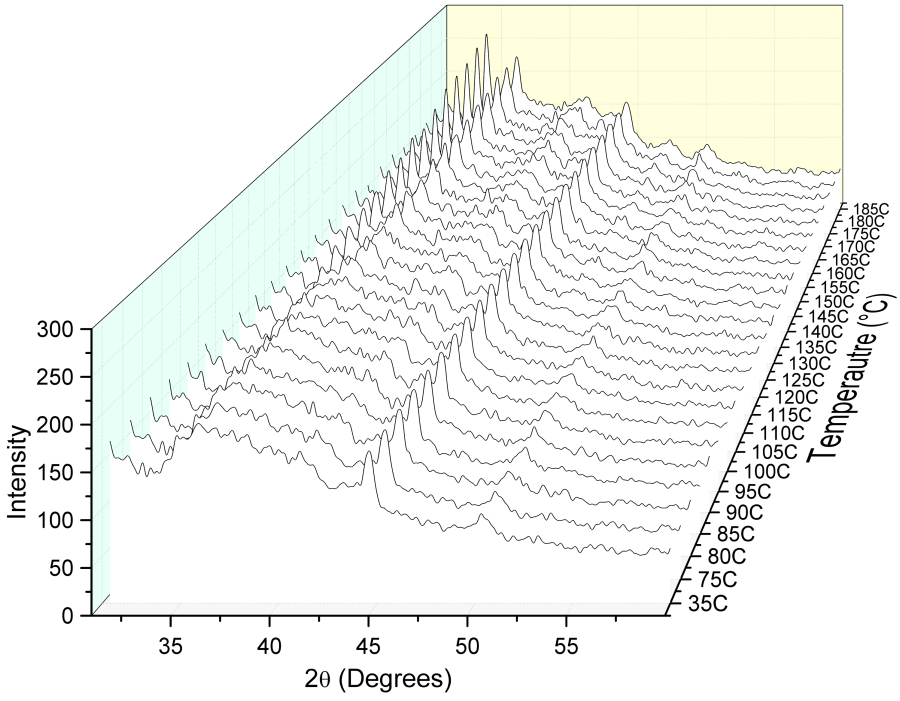


(b)

Figure 12: (a) Stacked XRD patterns from the incremental dynamic *in-situ* heating of film $Mg_{65}Zn_{30}Ca_5$. Note the peak around 51° is attributed to the AlN heating element, and the Al substrate peaks have been faceted as to not dwarf all other peaks. (b) The same XRD patterns as (a) presented in a cascading layout.

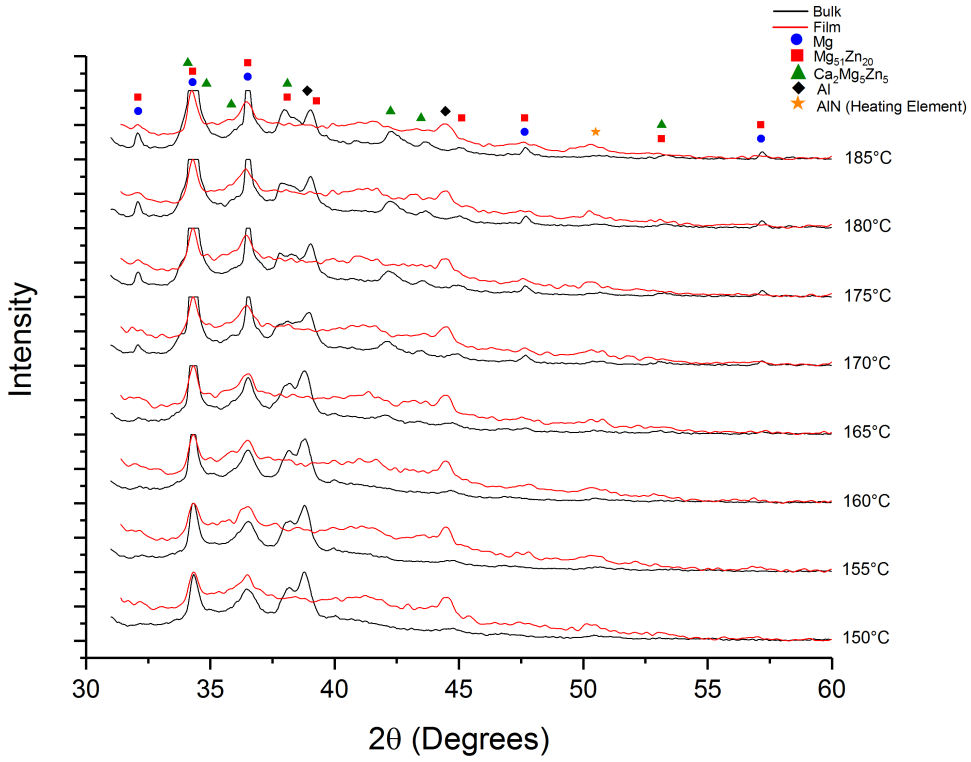


Figure 13: Normalised dynamic XRD from 150 – 185°C. Large bulk peaks have been faceted as to not dwarf smaller peaks and details.

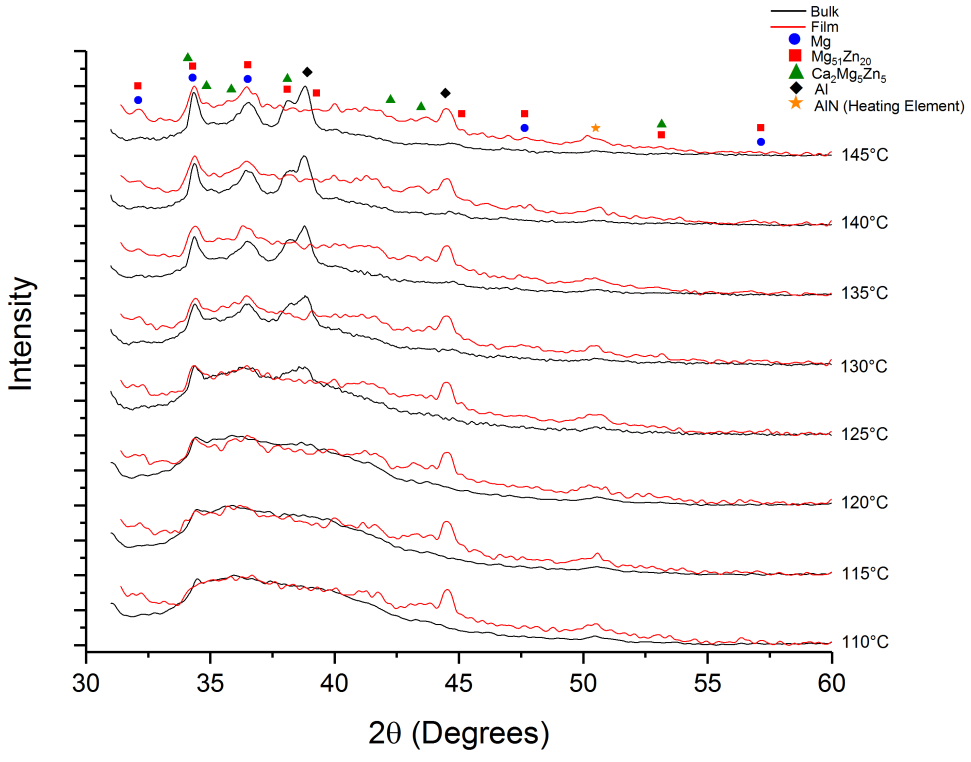


Figure 14: Normalised dynamic XRD from 110 – 145°C.

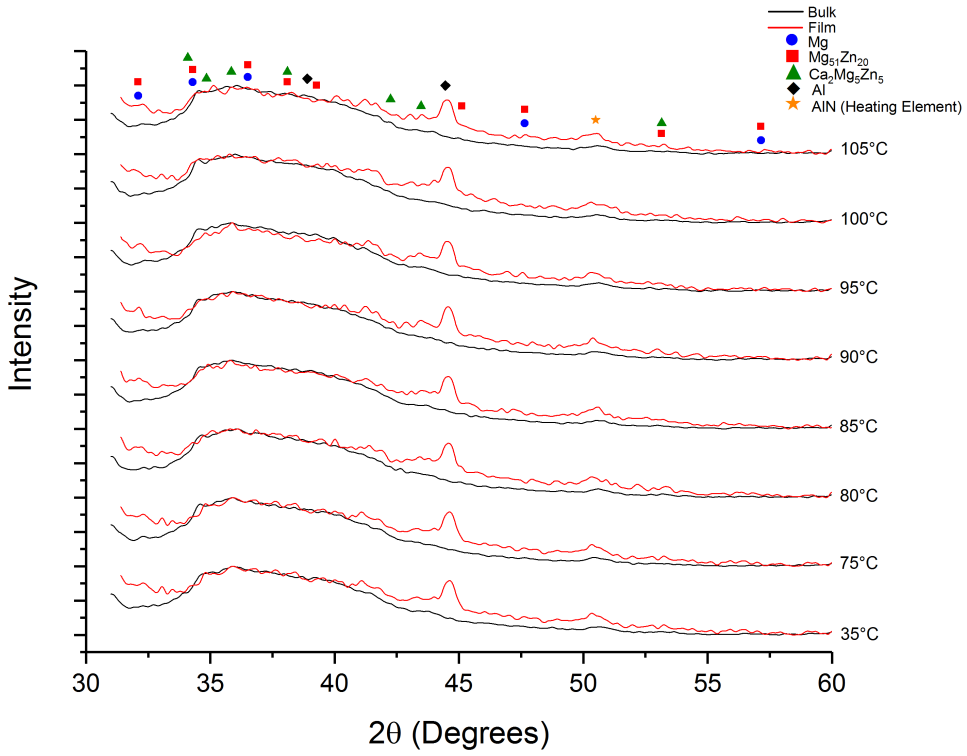


Figure 15: Normalised dynamic XRD from 35 – 105°C.

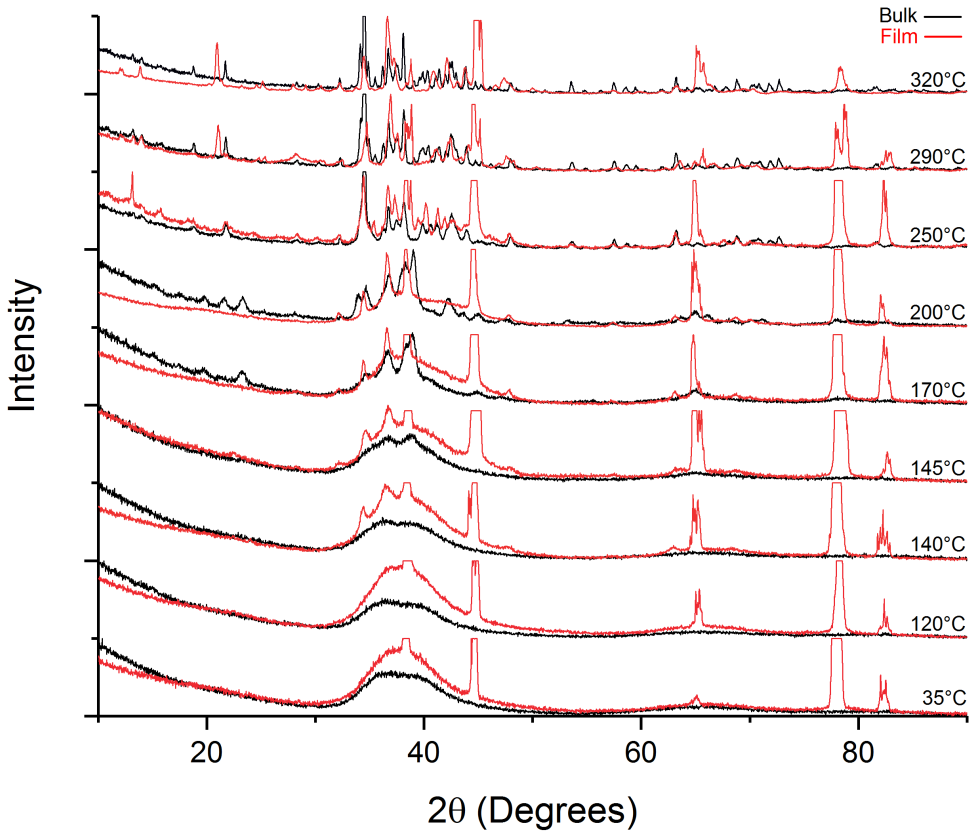


Figure 16: Supplementary: Normalised annealing XRD pattern for both bulk and film $Mg_{65}Zn_{30}Ca_5$ heated treated to several temperatures for crystallisation peak identified from DSC. Bulk is shown in black, and film in red. Note the Al substrate and other high intensity peaks have been faceted as to not dwarf all other peaks.

Table 9: Supplementary: Annealing XRD $2\theta$ peak pattern list. Peaks which appear in both the bulk and film are marked "Both," peaks only appearing on the bulk are marked "Bulk Only," and peaks only appearing on the film are marked "Film Only."

| Mg | | $Mg_{51}Zn_{20}$ | | $Ca_2Mg_5Zn_5$ | | $Ca_2Mg_5Zn_{13}$ | | MgZn | |
|---|---|---|---|---|---|---|---|---|---|
| 32.2640 | Both | 15.1461 | Bulk Only | 10.8738 | Both | 12.114 | Both | 12.6360 | Both |
| 34.5053 | Both | 17.5798 | Bulk Only | 14.0992 | Both | 13.935 | Both | 14.7520 | Both |
| 36.7065 | Both | 19.4290 | Both | 17.9698 | Both | 20.165 | Both | 20.639 | Both |
| 47.9250 | Both | 21.6753 | Bulk Only | 21.7787 | Both | 21.035 | Both | 22.263 | Both |
| 57.4721 | Both | 23.2049 | Bulk Only | 23.5826 | Both | 23.329 | Both | 23.580 | Both |
| 63.2000 | Both | 24.5533 | Film Only | 26.1221 | Both | 24.641 | Both | 28.871 | Both |
| 67.4268 | Both | 27.6680 | Bulk Only | 28.3477 | Both | 25.281 | Both | 32.054 | Both |
| 68.7541 | Both | 30.4946 | Bulk Only | 30.3272 | Both | 27.947 | Both | 33.797 | Both |
| 70.1210 | Both | 32.0757 | Bulk Only | 32.8866 | Both | 29.258 | Both | 34.743 | Both |
| 72.6686 | Both | 34.0114 | Both | 34.2311 | Both | 30.699 | Both | 35.892 | Both |
| 77.9616 | Both | 36.3948 | Both | 34.9708 | Bulk Only | 31.589 | Both | 37.121 | Both |
| 81.7143 | Both | 36.9487 | Bulk Only | 36.3289 | Both | 33.929 | Both | 38.101 | Both |
| | | 37.8181 | Both | 37.6976 | Both | 35.308 | Both | 39.312 | Both |
| | | 39.1701 | Both | 38.1445 | Both | 35.892 | Bulk Only | 40.416 | Both |
| | | 42.4369 | Both | 39.7631 | Both | 36.806 | Both | 41.989 | Both |
| | | 43.2937 | Both | 41.2057 | Both | 37.281 | Both | 42.824 | Both |
| | | 44.8168 | Both | 42.4410 | Both | 38.269 | Both | 43.917 | Both |
| | | 47.9318 | Both | 43.9276 | Both | 40.041 | Both | 47.046 | Both |
| | | 57.4692 | Both | 45.3071 | Both | 40.991 | Both | 48.376 | Both |
| | | 63.2267 | Both | 48.1674 | Both | 42.195 | Both | 49.498 | Both |
| | | 64.1349 | Film Only | 52.0808 | Both | 43.038 | Both | 51.285 | Both |
| | | 65.0419 | Bulk Only | 53.6599 | Both | 43.917 | Both | 53.211 | Both |
| | | 65.3533 | Film Only | 56.9387 | Both | 44.600 | Both | 55.660 | Both |
| | | 68.5726 | Bulk Only | 58.5610 | Both | 45.306 | Both | 57.955 | Both |
| | | 70.0382 | Both | 60.5081 | Both | 46.535 | Both | 60.026 | Both |
| | | 72.6234 | Both | 61.8530 | Both | 47.306 | Film Only | 62.260 | Both |
| | | 76.4763 | Bulk Only | 62.9999 | Both | 48.104 | Bulk Only | 63.687 | Both |
| | | 77.2025 | Bulk Only | 64.3501 | Both | 50.079 | Both | 65.186 | Both |
| | | 78.3347 | Both | 65.6320 | Both | 51.285 | Both | | |
| | | 82.0596 | Both | 66.8310 | Both | 56.178 | Bulk Only | | |
| | | | | 68.7827 | Both | 58.601 | Both | | |
| | | | | 70.1095 | Both | 59.940 | Both | | |
| | | | | 71.8163 | Both | 62.028 | Both | | |
| | | | | 72.8322 | Bulk Only | 63.590 | Both | | |
| | | | | 74.9981 | Both | 64.427 | Both | | |
| | | | | 78.0830 | Both | 66.229 | Both | | |
| | | | | 81.5094 | Bulk Only | 67.362 | Both | | |
| | | | | 82.6818 | Film Only | 68.198 | Both | | |
| | | | | 83.1204 | Both | 69.524 | Both | | |
| | | | | | | 70.480 | Both | | |
| | | | | | | 72.032 | Bulk Only | | |
| | | | | | | 73.329 | Both | | |
| | | | | | | 73.997 | Bulk Only | | |
| | | | | | | 76.736 | Both | | |
| | | | | | | 78.690 | Both | | |
| | | | | | | 79.631 | Both | | |

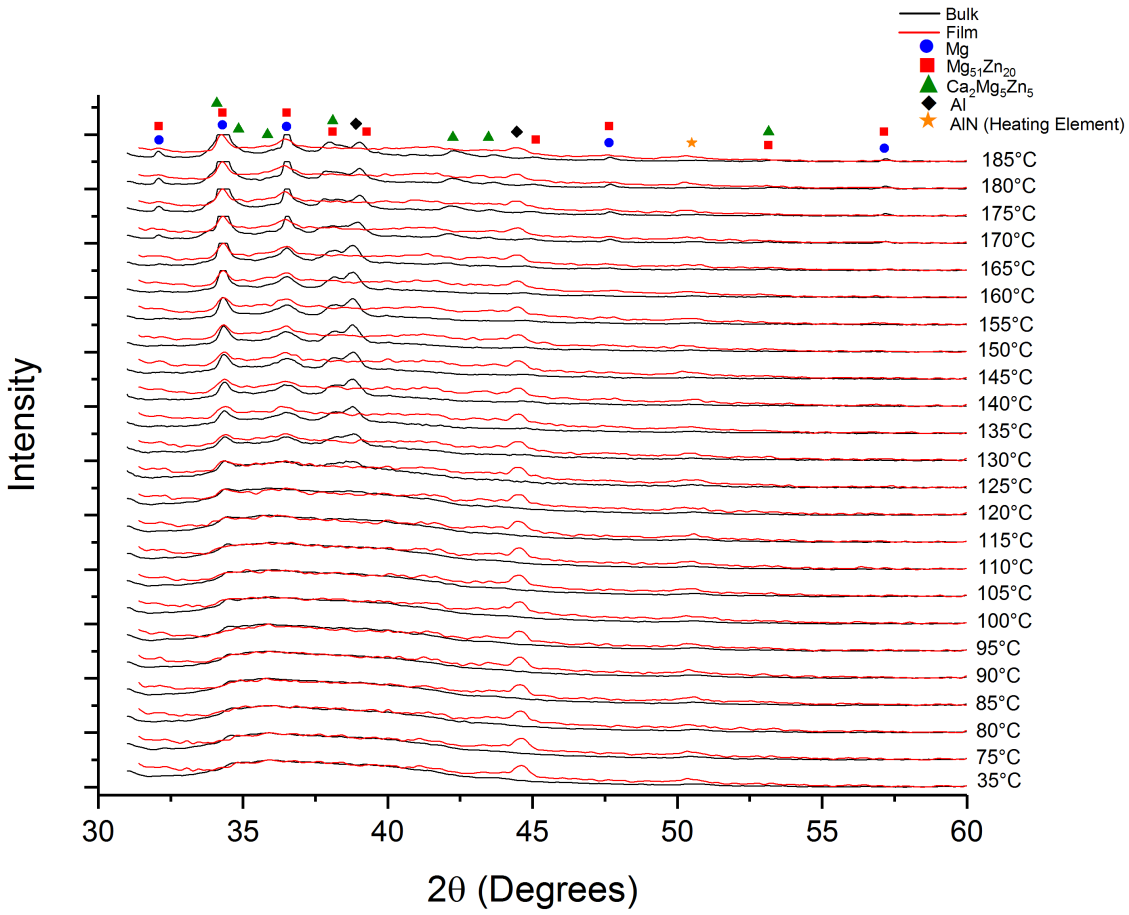


Figure 17: Supplementary: Normalised dynamic XRD pattern for both bulk and film $Mg_{65}Zn_{30}Ca_5$ heated incrementally *in-situ* from $35 - 185°C$ for crystallisation peak identified from DSC. Bulk is shown in black, and film in red. Note the Al substrate and other high intensity peaks have been faceted as to not dwarf all other peaks.